Noble Gas Clusters Doped with a Metal Ion I: Ab Initio Studies of Na^+Ar_n

Takeshi Nagata*

Department of Chemistry, Graduate School of Science, Hiroshima University, Higashi-Hiroshima 739−8526, and Computing and Communication Center, Kyushu University, Fukuoka 812-8581, Japan

Mutsumi Aoyagi

Computing and Communication Center, Kyushu University, Fukuoka 812-8581, Japan

Suehiro Iwata

National Institution for Academic Degrees and University Evaluation, Tokyo 187-8587, Japan

Received: August 15, 2003; In Final Form: October 19, 2003

The geometric structures and stability of Na^+Ar_n clusters were studied with ab initio molecular orbital methods. The clusters of $n = 6$, 8, and 10 have a high symmetry of O_h, D_{4d}, and D_{4d}, respectively. On the other hand, the clusters of $n = 3$ and 4 are deformed from the expected high symmetric configuration. It is the attractive force between rare gas atoms that breaks the symmetry. The many-body terms also play an important role in determining the detailed structures. The size dependence of the calculated thermochemical parameters are consistent with the reported mass spectral pattern which shows the first sequence of the magic number at $n = 6$ and 8.

Introduction

The physical and chemical properties of small atomic and molecular clusters have been the subject of intensive experimental and theoretical investigations in the last twenty years.[1−5] The number of atoms in clusters is between those of an isolated molecule and of bulk matter. The rapid progress in molecular beam techniques, in combination with laser evaporation techniques, allowed production of clusters for almost every element in the periodic table as well as their mixed clusters. The charged clusters are detected with time-of-flight (TOF) mass spectrometry. The intensity distribution of the spectrum reflects the stability of the clusters. The distribution shows often the irregular size dependence, and a few stronger peaks are found at the particular sizes rather than at neighboring sizes, suggesting that the clusters of those particular sizes are more stable than the others. The cluster sizes corresponding to such stable structures are called magic numbers. The sequences of the magic numbers found in the mass spectra are the fingerprints of the shell closure either of geometric or electronic structures, or both. Therefore, the observed sequences of magic number provide information on geometric and electronic structures of the clusters and thus on the interaction potential among the constituents of the clusters.

We report theoretical studies on noble gas clusters doped with a group 1 metal ion, M^+X_n, using ab initio molecular orbital (MO) methods. Recently, Velegrakis and co-workers [6−8] investigated those clusters both experimentally and theoretically. To analyze their observed mass spectral patterns, they performed the molecular dynamics (MD) simulation with empirical potential energy functions. However, the potential energy function used is simply the sum of the pair potentials. Besides, their pair wise potential function is Lennard-Jonnes type 6−12 functions both for ion−rare gas atom and for rare gas atom−rare gas atom. Because the small ion, such as the group 1 metal ion, strongly polarizes the surrounding rare gas atoms, it is expected that the interactions between the ion and a polarized atom and among polarized atoms are important; the former interaction leads to the $1/R^4$ dependence in the potential function and the latter results in many-body effects. In the present work, we examine the geometric structures and stability with more extensive ab initio MO methods.

In the structural model of Velegrakis et al.,[6] a simple hard sphere packing model is assumed to be applied for M^+X_n as for pure rare gas clusters; a central metal ion is surrounded by neutral atoms, and every additional atom occupies the position that offers the maximum number of neighbors until the atom−atom distances are too close to each other. For pure rare gas clusters X_n, with the hard sphere model the structure at the closure of the geometric shell is icosahedrons, and the sequence of the magic number is 13, 19, 23, 26, 29, 32....[6] So, if the ion radius of M^+ is comparable to the van der Waals radius of the noble gas X around M^+, the similar sequence of the magic number is expected for M^+X_{n-1}. In most cases, the ionic radius is not nearly equal to the van der Waals radius of the rare gas atom. If the hard sphere model can be applied yet, the stable geometric structures of M^+X_{n-1} are determined by the ratio of the ionic radius of the metal ion and the van der Waals radius of the rare gas atom. By assuming the close contact of the ion and atoms, the ratio

$$R^* \equiv R_{M^+-X}/R_{X-X} \leq \frac{1}{2}\left\{\frac{2 + \cos \pi/k - \cos 2\pi/k}{1 - \cos 2\pi/k}\right\}^{1/2} \quad (1)$$

provides the criteria of the stable geometric structure of the first shell.[6] Here, integer k is the number of rare gas atoms per ring and one of the two rings is twisted by an angle of π/k with

* Corresponding author. Address: Computing and Communication Center, Kyusyu University, Fukuoka 812-8581, Japan; e-mail: nagata@cc.kushida.kyushu-u.ac.jp; fax number: +81-92-642-2294.

10.1021/jp036443h CCC: $27.50
Published on Web 12/25/2003

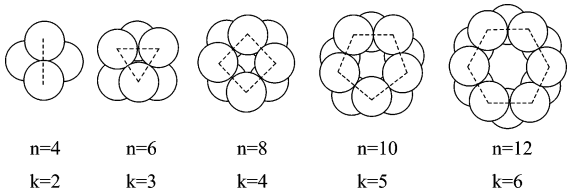

Figure 1. The geometrical model[6] of hard sphere packing model for clusters of the type MX_n.

respect to the other one; Figure 1 shows the schematic structures of the hard sphere clusters. When the ratio $R^* = R_{M+-X}/R_{X-X}$ is smaller than 0.6125 ($k = 2$), the geometry for the first closed shell is tetrahedron. For $0.6125 < R^* \leq 0.707$ ($k = 3$), $0.707 < R^* \leq 0.823$ ($k = 4$), $0.823 < R^* \leq 0.951$ ($k = 5$), and $0.951 < R^* \leq 1.088$ ($k = 6$), the corresponding geometries are octahedron (trigonal antiprism), square antiprism (SA), pentagonal antiprism (PA), and hexagonal antiprism (HA), respectively.[7] By adding an atom to the top and bottom of square of SA, the capped square antiprism (CSA) is a possible configuration under the hard sphere model.

The typical irregularity in the size dependence of the stability reflects the geometric and electronic structures and the interaction forces. In the experimental mass spectra, the magic number, where the irregularity is found, is determined, and then the structures might be able to be deduced using a model such as the hard sphere model. In the present study, with accurate ab initio calculations the size dependence of the geometric structures and thermochemical stability are examined. In this paper, we study Na^+Ar_n clusters, of which the ratio R_{Na^+-Ar}/R_{Ar-Ar} is 0.75 for the ionic radius of six coordinate ion and 0.80 for the ionic radius of eight coordinate ion.[9] It implies that it belongs to the SA region, independently on the ionic radius used. Experimentally, the mass spectrum reported by Lüder et al.[8] shows that the peaks at $n = 6$, 8, 10, 13, 16, and 20 are stronger than the neighboring n. In contrast to the mass distribution of Na^+Ar_n, the mass pattern of K^+Ar_n is rather monotonic[7] till $n = 10$ where the peak becomes substantially weaker than at $n = 9$, and the peaks at $n = 12$, 18, and 22 are stronger than the neighboring n.

Computational Details

The ionization energy of Na is much lower than that of Ar and therefore the charge is expected to reside on the Na atom. This implies that Na^+ and Ar atoms in Na^+Ar_n are electronically localized within its own ion and atoms, respectively. However, the cation Na^+ strongly polarizes the orbitals of argon atoms. Several basis sets for Na^+Ar were tested to select the proper basis set for further studies. The importance of polarization interaction will be examined in the next section. After a few test calculations, the 6-311++G(3df) basis set was selected. Polarization and dispersion interaction in this cluster are dominant for molecular interaction. Polarization interaction can be estimated with this basis set, and the dispersion interaction was evaluated by the second-order Møller−Plesset (MP2) perturbation theory. Basis set superposition error (BSSE)[9] in this basis set was examined, and it was shown that it can be almost neglected with the basis sets used.

At first, the initial geometries for Na^+Ar_n ($n = 2\sim10$) were determined using the hard sphere packing model. With the geometries optimized with the MP2(FULL)/6-311++G(3df), the vibrational analyses were carried out. Up to $n = 6$, the analytical calculations for vibrational analyses were possible. Since those for $n \geq 7$ were not feasible even on our supercomputer, the vibrational analyses were numerically calculated for those clusters. It was confirmed that all harmonic frequencies are real. Some of the small clusters had an imaginary frequency at a high-symmetry configuration, so that a careful re-optimization was required before reaching a real local minimum. Calculations for larger clusters were carried out on the VPP5000 at Research Center for Computational Science (RCCS), Okazaki National Research Institutes. Programs used are GAUSSIAN 98[11] registered at RCCS and MOLYX for LP SCF.[12]

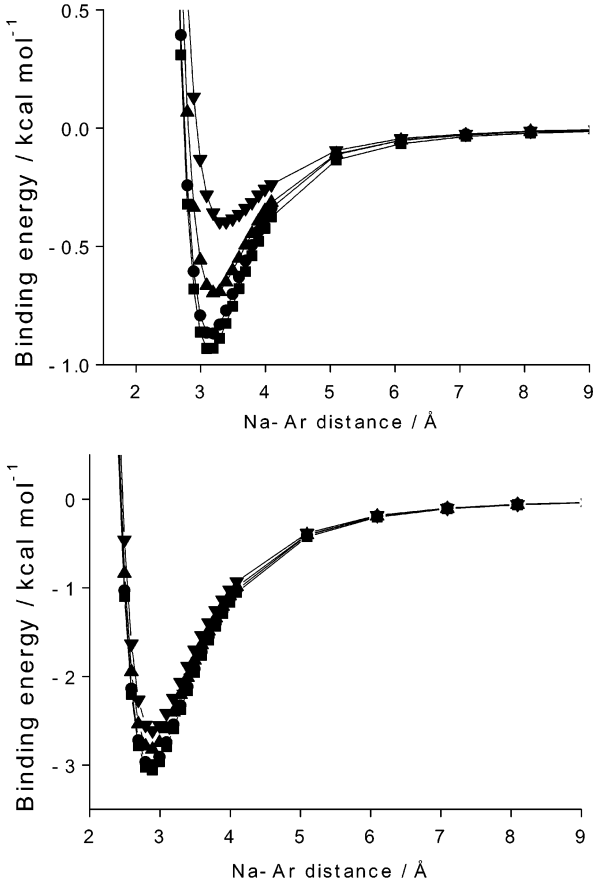

Figure 2. Potential energy curves of Na^+Ar in the SCF level of approximation. (a) With the 6-31++G basis set. (b) With the 6-311++G(3df). □: SCF without CP correction. ○: SCF with CP correction. △: locally projected SCF.[10] ▽: LP SCF with single excitation MP2.[14]

Results and Discussion

Polarization Interaction. First, we examine the levels of approximation to be used for the system. In their MD simulation, Prekas et al. used the (6,12) potential energy functions for the metal ion and a rare gas atom.[7] The form of the potential energy function is for the interaction between the neutral atoms. Because the ion induces the dipole moment (induced dipole moment) on the rare gas atom, it is expected that the interaction between the ion-induced dipole moment (the polarization interaction) plays a role in the cluster formation. To incorporate the polarization interaction in the calculations, we need to carefully examine the type of the basis sets. The potential energy curves in Figure 2a are calculated with the 6-31++G basis set, and those in Figure 2b are with the 6-311++G(3df) basis set, which contains the polarization functions. The binding energies are evaluated with the SCF level of approximation with and without the counterpoise (CP) correction.[13] In addition, the energies evaluated with the locally projected (LP) SCF method[10] and with the single excitation LP MP2 method[14] are shown in the figures. By adding the polarization functions, the binding

TABLE 1: Parameters of Murrel's Extended Rydberg Function for M^+Ar (M = Na, Li, K) and Ar_2

	Na^+Ar	Li^+Ar	K^+Ar	Ar_2
R_{eq}/Å	2.792	2.392	3.292	3.792
D_e^{ir}/kcal mol^{-1}	−4.078	−6.993	−2.428	−0.3206
a_1	1.699	1.675	1.469	2.170
a_2	−0.9914	−0.6835	−0.6565	-9.956×10^{-2}
a_3	0.7816	0.7865	0.6690	0.6099
a_4	−0.3381	−0.5378	−0.1987	9.931×10^{-2}
a_5	0.1651	0.3136	4.525×10^{-2}	-3.316×10^{-7}
a_6	-3.996×10^{-2}	-8.093×10^{-2}	-2.669×10^{-10}	
a_7	4.223×10^{-2}	8.784×10^{-3}		
a_8		1.765×10^{-10}		
b	1.689	1.861	1.660	2.268

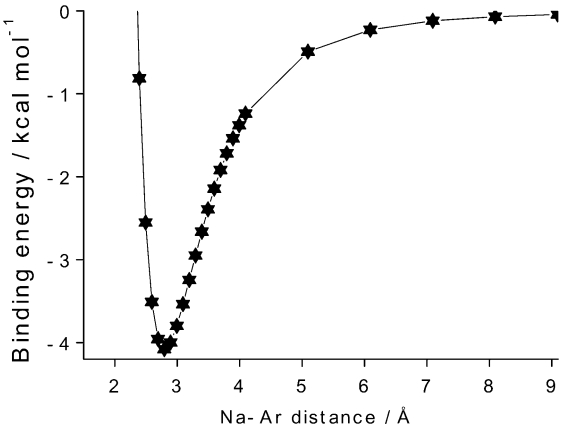

Figure 3. Potential energy curves of Na^+Ar. ▽: the 6-311++G(3df)/MP2 level of approximation. △: the extended Murrel function.

energy increases by more than 3 times: from 0.87 to 3.00 kcal/mol with the CP correction. Besides, the CP correction becomes very small with the 6-311++G(3df) basis set: 0.06 kcal/mol at the bottom of the curve.

As was previously demonstrated,[10] the LP SCF method, which is equivalent to SCF MI of Gianinetti,[15] underestimates the binding energy. This is particularly true for the smaller basis set. By adding the single excitation by the second-order perturbation method (LP MP2),[14] the curve becomes close to the CP corrected curve, particularly for the larger basis set. This is reasonable because the deficiency in the LP SCF (MI) method is a direct consequence from the neglect of the charge-transfer term, as proved analytically.[10] With the larger basis set, the energy differences among four curves are small compared with the total binding energy, which suggests that the charge-transfer term is not large; the charge-transfer energy at the infinite separation is the ionization energy difference of Ar and Na atoms, which is 10.62 eV.

The polarization interaction is thus taken into account in the SCF level of approximation by adding 3df functions to the basis set. Figure 3 shows the potential energy curve evaluated with the MP2 method (without the CP correction). The binding energy increases further, and the equilibrium bond distance is slightly shortened from 2.892 Å (SCF) to 2.792 Å (MP2). For qualitative discussion, the SCF method might be useful, but for quantitative analyses, the comparison of Figure 3 and Figure 2b indicates that the electron correlation should be included in the calculations. So, in the present study, the MP2(FULL)/6-311++G(3df) level of calculations are used for the geometry optimization as well as for the harmonic frequency calculation.

For further studies, the curve is fitted to an analytical function; we selected Murrel's extended Rydberg function,[16]

$$V(R) = D_e^{ir}(1 + \sum_{i=1} a_i\rho) \exp(-b\rho), \qquad (2)$$

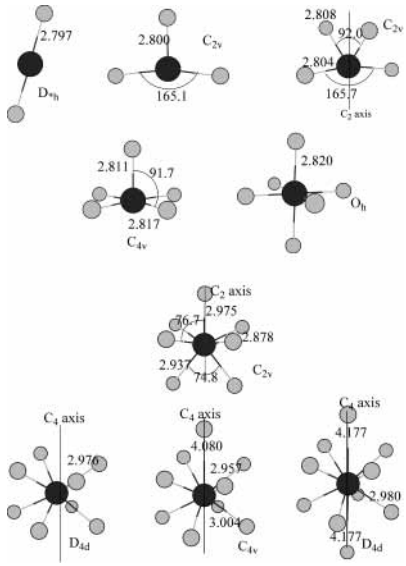

Figure 4. The geometries of Na^+Ar_n clusters ($n = 2\sim10$).

where $\rho = R - R_{eq}$, R_{eq} is the equilibrium bond distance and D_e^{ir} is the depth of potential. The coefficients a_i and b are optimized so that the error of the fitting becomes less than 0.02 kcal mol^{-1}. The fitting function converges at $i = 7$ for Na^+Ar molecule. Figure 3 shows ab initio result and its fitted curve. The similar successful fittings are attained for Li^+Ar and K^+-Ar as well as for Ar_2 with the same form of the function. The fitting parameters for these molecules are summarized in Table 1.

Magic Number Sequence and the Corresponding Geometry. In the hard sphere model, the ratio R_{Na^+-Ar}/R_{Ar-Ar} is within the SA region, which implies the first shell closure is $n = 8$ for Na^+Ar_n. By adding the atoms on the caps, the next magic number is $n = 10$ with the CSA structure. Experimentally, the reported magic number sequence for the Na^+Ar_n clusters is $n = 6, 8, 10, 16, 20, 23, 25, 26, 29....$[8] Thus, at least the hard sphere model is consistent with the second and third magic numbers at $n = 8$ and $n = 10$, but not for the first one. Since no experimental information on the geometric structures is available other than the mass spectral pattern, the full geometry optimization for the clusters with the ab initio MO calculations is essential in confirming the model.

Figure 4 shows the optimized geometries of Na^+Ar_n clusters. The equilibrium bond distances of $R(Na^+-Ar)$ and some of $R(Ar-Ar)$ are summarized in Table 2. Na^+Ar_2 has the $D_{\infty h}$ symmetry, and the equilibrium bond distance $R(Na^+-Ar)$ is close to that of the diatomic ion. Although all three $R(Na^+-Ar)$s in Na^+Ar_3 are 2.800 Å, three Ar atoms are not equivalent to each other and the geometry has the C_{2v} symmetry. The symmetry breaking of Na^+Ar_3 was unexpected. A careful recalculation of the harmonic frequencies at D_{3h} configuration

TABLE 2: The Bond Distances of Na^+-Ar and Ar−Ar

n	$R(Na^+-Ar)$	$R(Ar-Ar)$
1	2.794	
2	2.797	5.594
3	2.800, 2.800	4.209, 5.554
4	2.804, 2.808	4.038, 4.135, 5.564
5	2.811, 2.817	3.982, 4.038, 5.631
6	2.820	3.989, 5.641
7	2.878, 2.937, 2.975	3.568, 3.620, 3.635, 3.860, 4.063, 5.184, 5.599, 5.604
8	2.976	3.583, 3.675, 5.067, 5.627
9	2.957, 3.004, 4.080	3.565, 3.639, 3.656, 3.673, 5.042, 5.146, 5.631, 6.245
10	2.980, 4.177	3.617, 3.680, 3.634, 5.115, 5.631, 6.254

results in finding a pair of imaginary frequencies. For comparison, the geometries of Li^+Ar_3 and K^+Ar_3 are optimized; it turns out that Li^+Ar_3 is indeed in D_{3h}, while K^+Ar_3 has a nonplanar form of C_{3v}. We will discuss in the next subsection what causes these differences in the stable geometry, depending on the ionic radius.

With the hard sphere packing model, Na^+Ar_4 cluster can form a tetrahedral structure though the rare gas atoms are not at a close contact to each other. The geometry optimization starting from a tetrahedral geometry ends at a C_{2v} configuration shown in Figure 4; the C_2 axis is a bisector of two isosceles triangles formed by two pairs of Na^+Ar_2. The symmetry breaking takes place as in Na^+Ar_3. By addition of another rare gas atom to Na^+Ar_4, the geometry of Na^+Ar_5 is optimized, and it converges to a high-symmetry configuration of C_{4v}. Four argon atoms form a square and an extra atom is located on the C_4 axis. The geometry of the Na^+Ar_6 cluster is optimized from the octahedral conformation, which is guessed from the hard sphere packing model. This time, the octahedral conformation of O_h symmetry is at a true minimum and is very stable. It may be considered as a shell closure as discussed below.[6]

It was difficult to find a stable structure for Na^+Ar_7. So, we took a procedure inverted to the ordinal one; an atom is removed from the optimized Na^+Ar_8 cluster. As is shown in Figure 4, the geometry of Na^+Ar_7 is complicated, but it has relatively high symmetry (C_{2v}). Four atoms form approximately a square. The optimized geometry of the Na^+Ar_8 cluster is a square antiprism (SA) configuration as is guessed from the hard sphere packing model. It has D_{4d} symmetry with the C_4 axis passing through both centers of two pairs of squares. The Na^+Ar_9 conformer keeps the core of Na^+Ar_8, having an extra atom as a cap on the C_4 axis. The ninth atom may be regarded as the first member of the second shell.

The optimized geometry of the Na^+Ar_{10} cluster is the capped square antiprism (CSA) structure and has the D_{4d} symmetry as the Na^+Ar_8 cluster. It is not a pentagonal antiprism (PA). Two Na^+-Ar distances in the Na^+Ar_{10} cluster are 4.177 Å and much longer than the other Na^+-Ar ones (2.980 Å). The structure of Na^+Ar_{10} is formed by adding an atom at the other end of Na^+Ar_9.

Interaction Potential Energies. The symmetry of Na^+Ar_3 and Na^+Ar_4 at the equilibrium configuration is lower than the expected one as mentioned above. A simple hard sphere packing model fails in these small clusters. By analyzing the cause of the symmetry breaking, the factors which determine the stable geometry might be deduced. Because both Na^+ ion and Ar atoms are closed shell systems and the ionization energy difference of Na and Ar is large, the leading attractive force between a Na^+ ion and an Ar atom is the charge-induced dipole interaction, whose analytical form in the perturbation theory is $-\alpha_{Ar}/R^4$. To simulate the ab initio energy accurately, however, the interaction energy cannot be expanded simply in terms of the inverse of the bond distance R. We found that Murrel's extended Rydberg function gives the accurate fitting to the MP2 energy curve of Na^+ and Ar. Similarly, the same form of the function can be used for Ar−Ar interaction, although the (6, 12) function is traditionally extensively used.

The simplest way to estimate the interaction energy of Na^+-Ar_n is to assume the pair wise potential; the energy is

$$V^{\text{pair}}(Na^+Ar_n) = \sum_{j=1}^{n} V_{\text{ion-Ar}}(R_{Na^+-Ar^j}) + \sum_{j<k}^{n} V_{Ar-Ar}(R_{Ar^k-Ar^j}) \quad (3)$$

Figure 5a plots the energy $V^{\text{pair}}(Na^+Ar_3)$ for a planar configuration (Figure 5c); the parameters determined in the present study are used. Three of $R_{Na^+-Ar^j}$ is fixed at 2.800 Å. In the figure, the potential $V^{MP2}(Na^+Ar_3)$ with ab initio MP2(FULL)/6-311++G(3df) is also shown. Two curves have a saddle point at the angle $\theta = 120°$ of D_{3h} configuration. Both curves have two local minima, whose angles are summarized in Table 3. The difference of the two curves is given in Figure 5b, and it shows that the nonadditive many-body terms are positive. For comparison, the corresponding curves for Li^+Ar_3 and K^+Ar_3 are shown in Figures 6 and 7.[17] The positive many-body terms are small in absolute values by 1 order of magnitude for all three cases. The rough shape of the potential curves is determined by the pair wise interaction, but in details the angles at the minima are tuned by the many-body terms, in particular for the deeper minimum. The dominant many-body interaction is the interaction between the induced dipole moments on the rare gas atoms, which we discuss later.

Because the Na^+-Ar distance is fixed and therefore the ion−rare gas atom interaction is not dependent on the angle, the shape of the curve V^{pair} is determined by the Ar−Ar interaction potential V_{Ar-Ar}, which is attractive in Na^+Ar_3; the minimum of the function V_{Ar-Ar} is at 3.792 Å. This attractive interaction between Ar atoms explains the two minima of the curve V^{pair}. As shown in Table 3, at the deeper minimum, two short Ar−Ar distances are almost equal to the equilibrium distance in V_{Ar-Ar}, while at the shallower minimum there is only one short Ar−Ar pair. The shorter Ar−Ar distances in two local minima

TABLE 3: Angles ($\angle Ar^2MAr^3$, $\angle Ar^2MAr^1$) at Two Local Minima on $V^{\text{pair}}(M^+Ar_3)$ and $V^{MP2}(M^+Ar_3)$

		shallow			deep		
		$\angle Ar^2M\,Ar^3$	$\angle Ar^2M\,Ar^1$	$R(Ar-Ar)^a$	$\angle Ar^2M\,Ar^3$	$\angle Ar^2M\,Ar^1$	$R(Ar-Ar)^a$
Li^+Ar_3	V^{pair}	115°	122.5°	3.97, 4.13	145°	107.5°	4.49, 3.80
Li^+Ar_3	V^{MP2}				120°	120°	4.08
Na^+Ar_3	V^{pair}	85°	137.5°	3.78, 5.22	190°	8°	5.58, 3.78
Na^+Ar_3	V^{MP2}	95°	132.5°	4.13, 5.13	165°	97.5°	5.55, 3.78
K^+Ar_3	V^{pair}	70°	145°	3.72, 6.19	220°	70°	6.10, 3.72
K^+Ar_3	V^{MP2}	75°	142.5°	3.95, 6.15	210°	75°	6.27, 3.95

[a] The first number is $R(Ar^2-Ar^3)$ and the second is $R(Ar^2-Ar^1) = R(Ar^3-Ar^1)$.

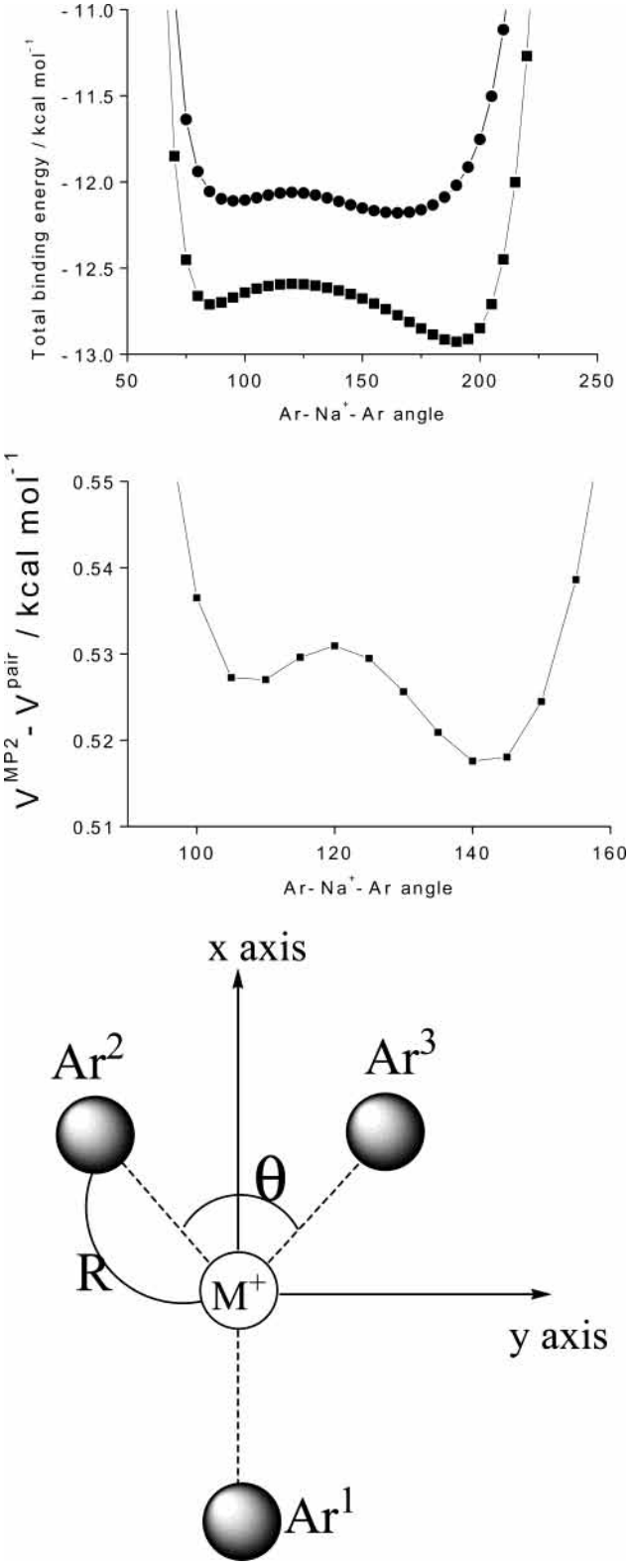

Figure 5. (a) The potential energy curves of Na^+Ar_3 as a function of the angle $\angle Ar^2NaAr^3$. All of the bond lengths R(Na−Ar) is fixed at 2.800 Å. ○: MP2/6-311++G(3df). □: $V^{pair}(Na^+Ar_3)$, a sum of the paired potential energy functions determined for diatomic molecules. (b) The difference $V^{MP2}(Na^+Ar_3) - V^{pair}(Na^+Ar_3)$. (c) The planar geometry of M^+Ar_3.

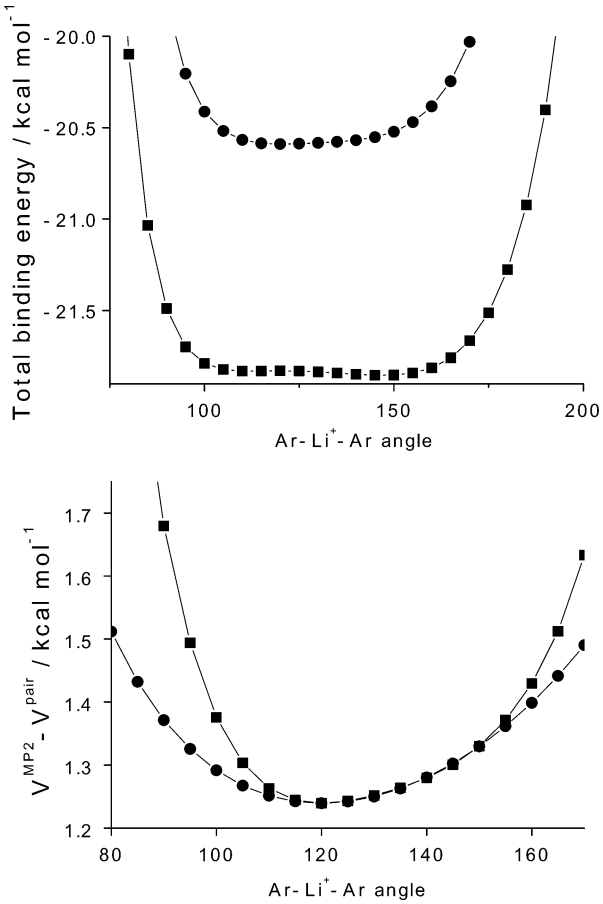

Figure 6. (a) The potential energy curves of Li^+Ar_3 as a function of the angle $\angle Ar^2LiAr^3$. All of the bond lengths R(Li−Ar) is fixed at 2.356 Å. ○: MP2/6-311++G(3df). □: $V^{pair}(Li^+Ar_3)$, a sum of the paired potential energy functions determined for diatomic molecules. (b) □: the difference $V^{MP2}(Li^+Ar_3) - V^{pair}(Li^+Ar_3)$. ○: a plot of eq 4.

are equal to each other. This is also true for K^+Ar_3. Both in Na^+Ar_3 and K^+Ar_3, the attractive interaction among three Ar atoms are so dominant that if the many-body terms are excluded, the metal ion is located outside of the triangle formed by three Ar atoms, as the angle $\angle Ar^2MAr^3$ at the deeper minimum is larger than 180°. With MP2 full geometry optimization for K^+-Ar_3 by removing the planar restriction, the ion lies on the top of an equilateral triangle of Ar_3, the geometry having C_{3v} symmetry and all three R_{Ar-Ar} being 3.949 Å,[17] equal to the shorter R_{Ar-Ar} at the local minima in the planar model.

For Li^+Ar_3, the situation is slightly different because of the small ionic radius of Li^+; the equilibrium distance of the diatomic ion Li^+Ar is 2.392 Å. The shorter Ar−Ar distance at the deep minimum is 3.800 Å and is almost equal to the corresponding distance in Na^+Ar_3. The Ar−Ar interaction is still attractive, but the angular dependence of V^{pair} is weak at $100° < \angle Ar^2MAr^3 < 150°$ as seen in Figure 6a.

The many-body (nonadditive) terms, which are estimated by the difference $V^{MP2} - V^{pair}$, are important in determining the true minimum of the potential energy surface, although the absolute value is small, which is seen in Figures 5b, 6b, and 7b. The terms at $\angle Ar^2MAr^3 = 120°$ are 1.23 kcal/mol for Li^+-Ar_3, 0.53 kcal/mol for Na^+Ar_3, and 0.18 kcal/mol for K^+Ar_3. With the ab initio MP2 calculation, the many-body terms contain various terms, including the electron delocalization over three or four atoms (ion). In the second-order perturbation theory for molecular interaction, the leading many-body term is supposed to be the induced dipole−induced dipole interaction. The induced dipole moment is proportional to α_{Ar}/R_{ion-Ar}^2. There-

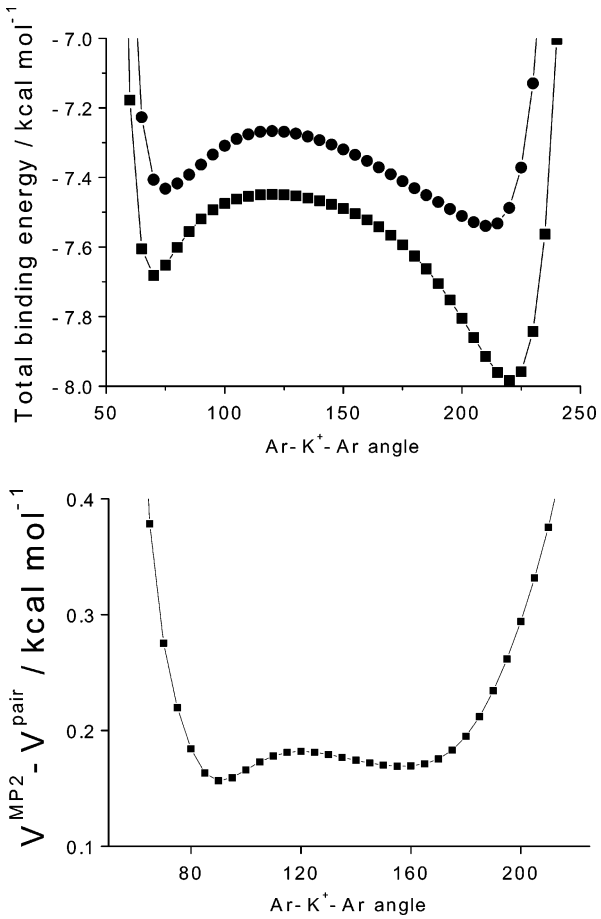

Figure 7. (a) The potential energy curves of K^+Ar_3 as a function of the angle $\angle Ar^2KAr^3$. All of the bond lengths $R(K-Ar)$ are fixed at 3.245 Å. ○: MP2/6-311++G(3df). □: $V^{pair}(K^+Ar_3)$, a sum of the paired potential energy functions determined for diatomic molecules. (b) The difference $V^{MP2}(K^+Ar_3) - V^{pair}(K^+Ar_3)$.

fore, the terms decrease with the ionic radius. In the present planar M^+Ar_3 model, the term is given as

$$V^{id-id}(R,\theta) = \frac{2}{R^3_{Ar^1-Ar^2}}\left\{\boldsymbol{\mu}_1\cdot\boldsymbol{\mu}_2 - 3\left(\boldsymbol{\mu}_1\cdot\frac{\mathbf{R}_{Ar^1-Ar^2}}{R_{Ar^1-Ar^2}}\right)\left(\boldsymbol{\mu}_2\cdot\frac{\mathbf{R}_{Ar^1-Ar^2}}{R_{Ar^1-Ar^2}}\right)\right\} + \frac{1}{R^3_{Ar^3-Ar^2}}\left\{\boldsymbol{\mu}_3\cdot\boldsymbol{\mu}_2 - 3\left(\boldsymbol{\mu}_3\cdot\frac{\mathbf{R}_{Ar^3-Ar^2}}{R_{Ar^3-Ar^2}}\right)\left(\boldsymbol{\mu}_2\cdot\frac{\mathbf{R}_{Ar^3-Ar^2}}{R_{Ar^3-Ar^2}}\right)\right\}$$

where the absolute-induced dipole moment is $|\boldsymbol{\mu}_i| = \alpha_{Ar}/R_{ion-Ar}^2$. For the model configuration in Figure 5c, the function can be written as

$$V_{id-id}/(\alpha_A^2/R^7) = \frac{3+\cos\frac{\theta}{2}}{\left(\sqrt{2\left(1+\cos\frac{\theta}{2}\right)}\right)^3} + \frac{1+\sin^2\frac{\theta}{2}}{8\sin^2\frac{\theta}{2}} \quad (4)$$

which has a single minimum at $\theta = 120°$. In Figure 6b, the function is plotted by assuming that $\alpha_A^2/R^7 = 1.23$ kcal/mol, which is determined as the plots of V^{id-id} and $V^{MP2} - V^{pair}$ coincide to each other at the bottom. Both plots have a minimum at $\theta = 120°$, and the curves are close to each other between 110° and 150°. Outside of these angles, where the distances between argon atoms are short, two curves differ very much. The difference is prominent for Na^+Ar_3 and K^+Ar_3 because $V^{MP2} - V^{pair}$ has two minima as is seen in Figure 5b and 7b. These differences imply that there are the many-body terms other than V^{id-id}, however small they are in absolute values. The ratio of $V^{MP2} - V^{pair}$ at $\theta = 120°$ for Li^+Ar_3, Na^+Ar_3, and K^+Ar_3 is 1.23:0.53:0.19 (kcal/mol) = 1:0.43:0.15, which deviates, although not very much, from the ratio of $1/R_{M+-Ar}^7$, $(1/2.356)^7$: $(1/2.800)^7$: $(1/3.245)^7 = 1:0.30:0.11$. Although further numerical and theoretical studies are required to identify the cause of the many-body interaction terms, the double minima in $V^{MP2} - V^{pair}$ for Na^+Ar_3 and K^+Ar_3, similar to V^{pair}, suggest that three-body terms among three argon atoms may contribute to it.

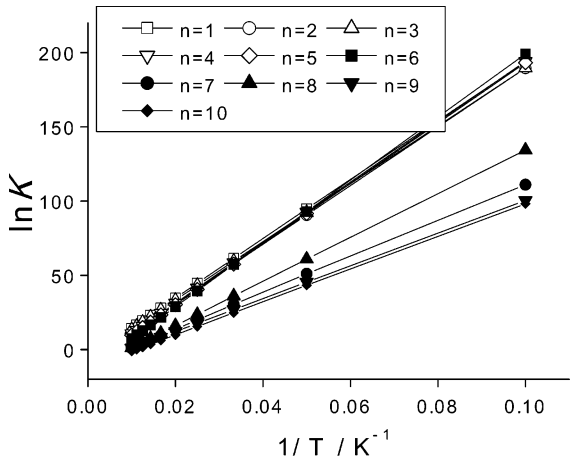

Figure 8. The van't Hoff plot of $Na^+Ar_{n-1} + Ar \rightarrow Na^+Ar_n$.

TABLE 4: The Total Energy Difference ($\Delta E_{n,n-1}$/kcal mol^{-1}) and Enthalpy and Entropy Changes ($\langle\Delta H_{n,n-1}\rangle$/kcal mol^{-1} and $\langle\Delta S_{n,n-1}\rangle$/cal K^{-1}mol^{-1}) in Reaction $Na^+Ar_{n-1} + Ar \rightarrow Na^+Ar_n$[a]

n	$\Delta E_{n,n-1}$	$\langle\Delta H_{n,n-1}\rangle$	$\langle\Delta S_{n,n-1}\rangle$
1	−4.08	−3.97	−10.75
2	−4.08	−3.94	−17.24
3	−4.02	−3.89	−11.77
4	−4.21	−4.05	−18.95
5	−4.19	−4.05	−20.96
6	−4.37	−4.23	−27.34
7	−2.60	−2.43	−21.73
8	−3.05	−2.94	−26.96
9	−2.28	−2.20	−19.83
10	−2.30	−2.19	−24.09

[a] The changes $\langle\Delta H_{n,n-1}\rangle = \langle H_n - H_{n-1}\rangle$ and $\langle\Delta S_{n,n-1}\rangle = \langle S_n - S_{n-1}\rangle$ are estimated with a least-squares fitting of eq 6.

Thermochemical Parameters and Magic Numbers of Na^+Ar_n Clusters. A few thermochemical parameters for an addition reaction of an Ar atom to Na^+Ar_{n-1},

$$Na^+Ar_{n-1} + Ar \rightarrow Na^+Ar_n \quad (5)$$

are evaluated using the calculated harmonic frequencies. The equilibrium constant K

$$\ln K = -\frac{\Delta G_{n,n-1}}{RT} = -\frac{\Delta H_{n,n-1}}{RT} + \frac{\Delta S_{n,n-1}}{R} \quad (6)$$

is estimated with the changes of Gibbs free energies ($\Delta G_{n,n-1}$), enthalpies ($\Delta H_{n,n-1}$), and entropies ($\Delta S_{n,n-1}$) between Na^+Ar_n and $Na^+Ar_{n-1} + Ar$. Figure 8 shows ln K plots versus $1/T$ between 10 and 100 K. They are all linear in this temperature region. It is because all of the vibrational modes have low frequencies; the largest for $n = 6$ is 146 cm^{-1}. In Table 4, the least-squares fitted $\langle\Delta H_{n,n-1}\rangle$ and $\langle\Delta S_{n,n-1}\rangle$ are given; they are practically equal to $\Delta H_{n,n-1}{}^{50K}$ and $\Delta S_{n,n-1}{}^{50K}$. In the table, the

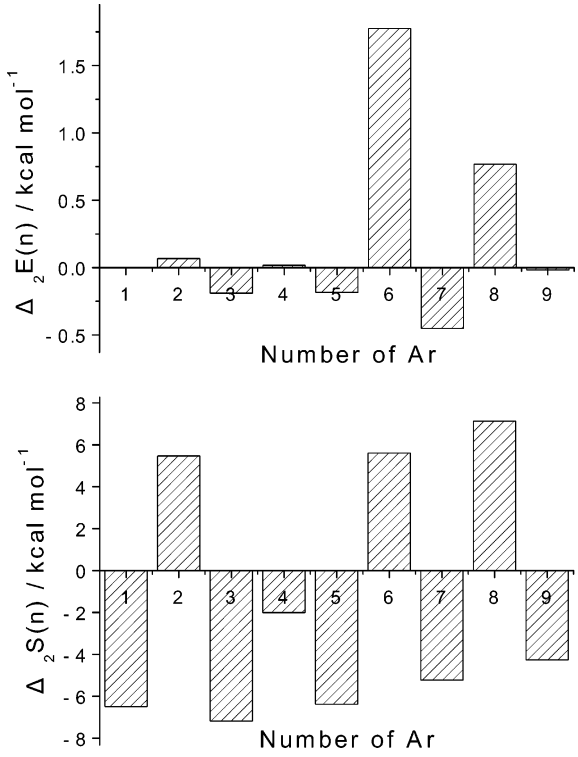

Figure 9. Bar graphs representing the second differences defined in 7. (a) $\Delta_2E(N)$, (b) $\Delta_2S(N)$.

incremental binding energy $\Delta E_{n,n-1}$ is also given, which is in parallel with $\Delta H_{n,n-1}$. For $n = 1-6$, the lines almost coincide with each other. The slopes of the line for $n = 7$, 9, and 10 are much smaller than those for $n \leq 6$, while that for $n = 8$ is between them. It is the geometric changes that reflect the incremental enthalpy change $\Delta H_{n,n-1}$ and binding energy change $\Delta E_{n,n-1}$ at $n = 7$. The octahedral Na^+Ar_6 is very stable, and $\langle \Delta H_{n,n-1} \rangle$ for $n = 6$ is the largest -4.23 kcal mol^{-1} among the calculated ones. There are 12 of the attractive short Ar−Ar pairs, and their distance is as short as for $n = 5$ (see Table 2). For $n = 7$, on the other hand, the ion−argon distances increase because of the congestion of argon atoms, which is seen in the shorter Ar−Ar distances than R_{eq} of Ar_2 as shown in Table 2. So the stability gain by adding an atom is small.

The incremental enthalpy change slightly increases for $n = 8$, although the ion−argon distances are further lengthened. The structure is SA. For Na^+Ar_9, an atom is on the top of cap, far apart from the ionic center Na^+. The capping Ar atom is regarded as the first member belonging to the second shell. The change $\langle \Delta H_{9,8} \rangle$ is smaller than $\langle \Delta H_{7,6} \rangle$. By adding one more cap to Na^+Ar_9, Na^+Ar_{10} of CSA configuration is formed; the change $\langle \Delta H_{10,9} \rangle$ is nearly equal to $\langle \Delta H_{9,8} \rangle$.

To compare the above results with the results calculated using the MD simulation by Prekas et al.,[7] the second difference of the total energy $\Delta_2E(N)$, defined as

$$\Delta_2E(N) = E(n+1) + E(n-1) - 2E(n) \qquad (7)$$

is evaluated and is shown in Figure 9, along with the second difference of entropy change. Both diagrams show clear distinction at $n = 6$ and 8, where the geometric shell closes by forming the octahedral (triangle antiprism) and square antiprism configuration. This is consistent with the reported mass spectrum,[8] which shows the relatively stronger peaks at $n = 6$, 8, and 10 than at the neighboring n, although we have not evaluated $\Delta_2E(10)$.

In their MD simulation, Prekas et al. used the ratio $R^* \equiv R_{M^+-X}/R_{X-X}$ and $\epsilon^* \equiv \epsilon_{M^+-X}/\epsilon_{X-X}$ as parameters, where ϵ is the parameter of the (6, 12) function. They showed the R^* and ϵ^* dependence of $\Delta_2E(N)$. Although the ratio is 0.75 (or 0.80) for Na^+Ar_n, our calculated $\Delta_2E(N)$ is more similar to their $\Delta_2E(N)$ for $R^* = 0.73$ than for $R^* = 0.75$ with $\epsilon^* = 10$. In the MD, there is a clear difference in $\Delta_2E(N)$ for the two R^*; for $R^* = 0.73$, $\Delta_2E(6)$ is about twice as large as $\Delta_2E(8)$, as in our calculated $\Delta_2E(N)$ in Figure 9. On the other hand, for $R^* = 0.75$, $\Delta_2E(6)$ is about a half of $\Delta_2E(8)$. Probably because the potential energy function of $\epsilon^* = 10$ is weaker for the ion−rare gas atom in the MD than ours, $\Delta_2E(N)$ by the simulation with the apparent smaller ionic radius (thus smaller R^*) becomes similar to our $\Delta_2E(N)$. In our calculations, the difference of $\Delta_2E(6)$ and $\Delta_2E(8)$ results from the extra stability of the octahedron (trigonal antiprism) structure of Na^+Ar_6, in which all of equivalent argon atoms are attractive to each other. On the other hand, in the square antiprism structure of Na^+Ar_8, even for the longer Na^+-Ar distance, there are too close Ar−Ar pairs, whose distance is 3.583 Å, shorter than R_{eq}(= 3.792 Å) of Ar_2; the Ar−Ar distance is at the repulsive wall of the potential energy function.

Conclusion and Future Works

For Na^+Ar_n clusters in our ab initio calculations, the large stability changes are at $n = 6$ and 8, which is consistent with the characteristics of the reported mass spectrum pattern. They correspond to the compact geometric structure of trigonal and square antiprisms (TA and SA). The attractive interaction among rare gas atoms plays an important role in determining the geometric structure, though if too congested, the interaction becomes repulsive. In the absolute values, the pair wise interaction dominates most of the binding energy, but the detailed analysis of the symmetry breaking of M^+Ar_3 (M = Li, Na, and K) reveals that the many-body interaction is important in determining the geometric structure. The induced dipole−induced dipole interaction is dominant in the many-body terms, but there are extra terms. Detailed investigations are needed by using the energy decomposition schemes[18−20] in the correlated level of theories. Our locally projected perturbation expansion can be applied for the analysis.[14] In our estimation for thermochemical parameters, the harmonic approximation is used but it is expected to be a crude approximation. In future works, molecular dynamics with accurate many-body potential energy functions should be carried out. As shown in M^+Ar_3, the comparison with the clusters Li^+Ar_n and K^+Ar_n are interesting even for the most stable conformation. In particular, the interaction among argon atoms is dominant in K^+Ar_n, which might be related to the observed difference in the mass patterns in Na^+Ar_n and K^+Ar_n. Clusters with various values of R^* rather than boundaries should be studied with more realistic many-body interaction energy functions.

Acknowledgment. We enjoyed talking with Prof. J. Lisy at the early stage of the work. T.N. thanks Prof. K. Saito of Hiroshima University for his encouragement. The work is partially supported by the Grant-in-Aids for Science Research (No. 11166270 and 11640518) by the Ministry of Education, Sports, and Culture, Japan, and for the Future "Photoscience" (JSPS-RFTF-98P01202) from Japan Society for the Promotion of Science. It is also a part of the works under the project "Computational Chemistry of Molecules in the Atmospheric Environment" of Research and Development Applying Advanced Computational Science and Technology under Japan

Science and Technology Corporation. A part of computations was carried out at Research Center for Computational Science, Okazaki National Research Institutes.

References and Notes

(1) Jena, P.; Khanna, S. N.; Rao, B. K. *Physics and Chemistry of Finite Systems*: *From Clasters to Crystals*; NATO ASI Ser. I, II; Kluwer Academic Publishers: Heidelberg, 1992.

(2) Haberland, H. *Clusters of Atoms and Molecules I, II*; Springer-Verlag: Berlin Heidelberg, 1995.

(3) Duncan, M. A. *Advances in Metal and Semiconductor Clusters 1, Spectroscopy and Dynamics*; Elsevier Science: Amsterdam, 1993.

(4) Duncan, M. A. *Advances in Metal and Semiconductor Clusters 2, Cluster Reactions*; Elsevier Science: Amsterdam, 1994.

(5) Duncan, M. A. *Advances in Metal and Semiconductor Clusters 3, Spectroscopy and Structure*; Elsevier Science: Amsterdam, 1994.

(6) Velegrakis, M. *Adv. Metal Semiconductor Clusters* **2001**, *5*, 227.

(7) Prekas, D.; Lüder, C.; Velegrakis, M. *J. Chem. Phys.* **1998**, *108*, 4450.

(8) Lüder, C.; Prekas, D.; Velegrakis, M. *Laser Chem*. **1997**, *17*, 109.

(9) *Kagaku Jiten* (in Japanese); Ohki, M., Ed.; Tokyo Kagaku Dojin: Tokyo, 1994; 104.

(10) Nagata, T.; Takahashi, O.; Saito, K.; Iwata, S. *J. Chem. Phys.* **2001**, *115*, 3553.

(11) Frisch, M. J.; Trucks, G. W.; Schlegel, H. B.; Scuseria, G. E.; Robb, M. A.; Cheeseman, J. R.; Zakrzewski, V. G.; Montgomery, J. A., Jr.; Stratmann, R. E.; Burant, J. C.; Dapprich, S.; Millam, J. M.; Daniels, A. D.; Kudin, K. N.; Strain, M. C.; Farkas, O.; Tomasi, J.; Barone, V.; Cossi, M.; Cammi, R.; Mennucci, B.; Pomelli, C.; Adamo, C.; Clifford, S.; Ochterski, J.; Petersson, G. A.; Ayala, P. Y.; Cui, Q.; Morokuma, K.; Salvador, P.; Dannenberg, J. J.; Malick, D. K.; Rabuck, A. D.; Raghavachari, K.; Foresman, J. B.; Cioslowski, J.; Ortiz, J. V.; Baboul, A. G.; Stefanov, B. B.; Liu, G.; Liashenko, A.; Piskorz, P.; Komaromi, I.; Gomperts, R.; Martin, R. L.; Fox, D. J.; Keith, T.; Al-Laham, M. A.; Peng, C. Y.; Nanayakkara, A.; Challacombe, M.; Gill, P. M. W.; Johnson, B.; Chen, W.; Wong, M. W.; Andres, J. L.; Gonzalez, C.; Head-Gordon, M.; Replogle, E. S.; Pople, J. A. *Gaussian 98*, revision A. 11; Gaussian, Inc.: Pittsburgh, PA, 1998.

(12) Developed by S. Iwata and his collaborators, http://hera.ims.ac.jp.

(13) Boys, S. F.; Bernardi, F. *Mol. Phys.* **1970**, *19*, 553.

(14) Nagata, T.; Iwata, S. *J. Chem. Phys.* **2004**, 120, in press.

(15) Gianinetti, E.; Vandoni, I.; Famulari, A.; Raimondi, M. *Adv. Quantum Chem.* **1998**, *31*, 251.

(16) Sorbie, K. S.; Murrel, J. N. *Mol. Phys.* **1975**, *29*, 1387.

(17) Nagata, T.; Aoyagi, M.; Iwata, S. in preparation.

(18) Jeziorski, B.; Moszynski, R.; Szalewicz, K. *Chem. Rev.* **1994**, *94*, 1887.

(19) Shütz, M.; Rauhut, G.; Werner, H.-J. *J. Phys. Chem. A* **1998**, *102*, 5997.

(20) Hamza, A.; Vibók, Á.; Halász, G. J.; Mayer, I. *Theor. Chem. Acc.* **2001**, *107*, 38.